

# Nanosecond Imaging of Microboiling Behavior on Pulsed-Heated Au Films Modified with Hydrophilic and Hydrophobic Self-Assembled Monolayers

Karin M. Balss,<sup>†</sup> C. Thomas Avedisian,<sup>\*,‡</sup> Richard E. Cavicchi,<sup>†</sup> and Michael J. Tarlov<sup>†</sup>

*Chemical Science and Technology Laboratory, National Institute of Standards and Technology, 100 Bureau Drive, Gaithersburg, Maryland 20899, and Sibley School of Mechanical and Aerospace Engineering, Cornell University, Ithaca, New York 14853*

*Received December 28, 2004. In Final Form: May 13, 2005*

Fast transient microboiling has been characterized on modified gold microheaters using a novel laser strobe microscopy technique. Microheater surfaces of different hydrophobicity were prepared using self-assembled monolayers of hexadecane thiol (hydrophobic) and 16-mercaptohexadecanol (hydrophilic) as well as the naturally hydrophilic bare gold surface. The microheater was immersed in a pool of water, and a 5- $\mu$ s voltage pulse to the heater was applied, causing superheating of the water and nucleation of a vapor bubble on the heater surface. Light from a pulsed Nd:Yag laser was configured to illuminate and image the sample through a microscope assembly. The timing of the short duration (7.5 ns) laser flash was varied with respect to the voltage pulse applied to the heater to create a series of images illuminated by the flash of the laser. These images were correlated with the transient resistance change of the heater both during and after the voltage pulse. It was found that hydrophobic surfaces produced a bubble that nucleated at an earlier time, grew more slowly to a smaller maximum size, and collapsed more rapidly than bubbles formed on hydrophilic surfaces.

## Introduction

When a solid surface is immersed in a liquid and heated at rates of several hundred million degrees per second, bubble nucleation can occur at superheat conditions close to predictions of homogeneous nucleation theory.<sup>1–5</sup> Such rapid evaporation at the superheat limit occurs in thermal ink-jet printing processes,<sup>1</sup> and it has been explored for its potential to move fluids in microfluidic devices.<sup>6,7</sup> In these applications, bubble morphology and growth rate determine the effectiveness of phase change to control the process under consideration. Since bubble nucleation at the superheat limit typically occurs on the order of microseconds for pure fluids at pressures near atmospheric, the ability to resolve time down to nanoseconds is required to capture details of the bubble morphology during rapid evaporation. This requirement is beyond the state-of-the-art for commercial instrumentation.

In this study, we use a new laser strobe microscopy technique for high temporal resolution imaging of fast transient microboiling events on microscale metallic heaters to investigate the influence of surface wetting on bubble dynamics. The technique improves upon previous attempts to visualize bubble formation on pulse-heated

microwires,<sup>3,8,9</sup> which produced images that were limited in temporal resolution by the duration of xenon flashlamps used for imaging, on the order of 500 ns, or of order 30 ns when using a laser diode for illumination. In our method, we couple a light pulse from a Nd:Yag laser (flash duration of 7.5 ns) with a microscope to produce time sequences of the fast nucleation and growth process.

The targeted applications are those where bubble growth occurs in a time-dependent temperature field associated with an impulsively heated thin metal film: the substrate surface temperature is not constant during growth. This situation significantly complicates quantitative analysis. However, it is emphasized that practical application motivates the present work—thermal ink-jet printing and sensing technologies—and they are based on operation precisely under these transient conditions. The heating pulse width of interest to this study—5  $\mu$ s—is dictated by the targeted applications.

Bubble morphology is strongly dependent on such factors as surface wetting, substrate surface temperature, fluid properties, and ambient conditions (pressure or temperature). Of these, surface wetting is the least understood. It is well known that wettability influences incipient nucleation temperature through contact angle even at high superheats typical of pulsed heating<sup>1,4</sup> as well as at more moderate conditions of nucleate boiling. All prior investigations of superheat and wettability examined the influence of wettability by altering either liquid properties or surface material (e.g., Teflon compared to glass). The notion of influencing bubble morphology by changing surface chemistry has not previously been addressed. Self-assembled monolayers (SAMs) offer this capability to change surface chemistry, superheat tem-

\* To whom correspondence should be addressed. E-mail: cta2@cornell.edu.

<sup>†</sup> National Institute of Standards and Technology.

<sup>‡</sup> Cornell University.

(1) Avedisian, C. T.; Osborne, W. S.; McLeod, F. D.; Curley, C. M. *Proc. R. Soc. London A* **1999**, *455*, 3875–3899.

(2) Avedisian, C. T. *J. Phys. Chem. Ref. Data* **1985**, *14* (3), 695–720.

(3) Skripov, S. *Superheated Liquids*; Hemisphere Publishing Co.: 1974; pp 113, 169–171.

(4) Thomas, O. C.; Cavicchi, R. E.; Tarlov, M. J. *Langmuir* **2003**, *19*, 6168–6177.

(5) Avedisian, C. T. *1986 Encyclopedia of Fluid Mechanics*; Gulf Publishing Co.: 1986; pp 130–190.

(6) Jun, T. K.; Kim, C. J. *J. Appl. Phys.* **1998**, *83*, 5658–5664.

(7) Geng, X.; Yuan, H.; Oguz, H. N.; Prosperetti, A. *J. Micromech. Microeng.* **2001**, *11*, 270–276.

(8) Glod, S.; Poulidakos, D.; Zhao, Z.; Yadigaroglu, G. *Int. J. Heat Mass Transfer* **2002**, *45*, 367–379.

(9) Hong, Y.; Ashgriz, N.; Andrews, J. *J. Heat Transfer* **2004**, *126*, 259–271.

perature, and bubble morphology for a given liquid and substrate material.

Recent interest in SAMs in such technological applications as chemical and biological sensing,<sup>10,11</sup> chemical resists in lithography,<sup>12,13</sup> corrosion protection, and molecular electronics<sup>14,15</sup> motivated Thomas et al.<sup>4</sup> to study the effect of SAMs on bubble nucleation temperature. SAMs were grown on gold-coated platinum microheaters to produce hydrophilic or hydrophobic monolayers (the conventional definition of a hydrophobic or hydrophilic surface is based on the contact angle (measured in the liquid) being greater or less than 90°, respectively).

A programmed voltage pulse was used to resistively heat the metal, and it produced a nucleation event that was detected by an inflection point in the evolution of electrical resistance that corresponded to predictions of homogeneous nucleation theory in the experiments previously reported. The temperature at these inflection points indicated that the heating rates were high enough to produce homogeneous nucleation, according to predictions of the theory.

Microheaters modified with hydrophobic SAMs exhibited lower but more pronounced inflection-point temperatures compared to those coated with hydrophilic SAMs. This difference was attributed to the lower effective contact angle for the hydrophobic SAM, which in turn would lower the nucleation temperature. The study showed that a single molecular layer can exert a strong influence on bubble nucleation. The bubble morphology was not examined because of the unavailability of optical diagnostics to probe the test surfaces on the relevant physical and temporal scales of the nucleation process. In the present work, we use SAMs to alter surface chemistry from the extremes of hydrophobic and hydrophilic on gold-coated platinum microheaters. The behavior of the bubbles observed on the heaters during and after the pulse are monitored and related to the thermal transients that are observed.

## Experimental Section

**Heater and Monolayer Preparation.** The microheaters were fabricated at Lincoln Laboratories and consisted of Au-coated Pt heaters in a layered structure shown in Figure 1a. The Pt heaters were rectangular, 15 μm wide, 30 μm long, and 200 nm thick. They were fabricated on a Si substrate with a 200-nm SiO<sub>2</sub> layer for thermal insulation and a 30-nm Ti layer for adhesion. The platinum surface was electroplated with a Au coating by immersing the microheaters in Bright Electroless Gold solution (Transene Co.)<sup>16</sup> at a bias of -2.2 V relative to ground for 1 min. The plating process was typically stopped within 3 min. The room-temperature resistance of the gold-coated heater was 3.2 Ω. By use of the bulk resistivities for gold and platinum, the thickness of the gold layer on this device is estimated to be about 35 nm. The heaters were connected to larger Pt wirebond pads for incorporation into the bridge assembly illustrated in Figure 1b.

(10) Tour, J. M.; Jones, L. II; Pearson, D. L.; Lamba, J. J. S.; Burgin, T. P.; Whitesides, G. M.; Allara, D. L.; Parikh, A. N.; Atre, S. V. *J. Am. Chem. Soc.* **1995**, *117*, 9529–9534.

(11) Prime, K. L.; Whitesides, G. M. *J. Am. Chem. Soc.* **1993**, *115*, 10714–10721.

(12) Kumar A.; Abbott N. L.; Kim E.; Biebuyck H. A.; Whitesides G. M. *Acc. Chem. Res.* **1995**, *28*, 219–226.

(13) Tarlov, M. J.; Burgess, D. R. F.; Gillen G. *J. Am. Chem. Soc.* **1994**, *115*, 5305–5306.

(14) Dhirani, A. A.; Zehner, R. W.; Hsung, R. P.; Guyotsonnest, P.; Sita, L. R. *J. Am. Chem. Soc.* **1996**, *118*, 3319–3320.

(15) Zehner, R. W.; Sita, L. R. *Langmuir* **1997**, *13*, 2973–2979.

(16) Certain commercial instruments are identified to adequately specify the experimental procedure. In no case does such identification imply endorsement by the National Institute of Standards and Technology.

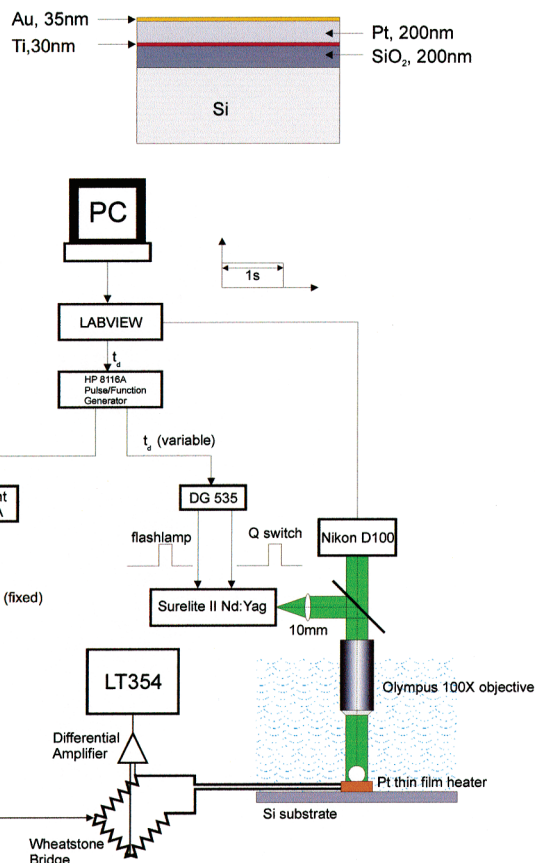


**Figure 1.** (a) Geometry of the heater structure. (b) Schematic of the experimental arrangement.

SAMs of hexadecanethiol (HDT) and 16-mercaptohexadecanol (HDOH) were prepared by immersing the heater in 1 mmol/L ethanolic solutions for 12 h. The heater was then rinsed with ethanol and dried with nitrogen before use. The Au film was cleaned and regenerated by ozone cleaning for 20 min, rinsing with ethanol, and drying with nitrogen. We refer to this surface condition as bare Au. These treatments are known to produce hydrophobic and hydrophilic surfaces based on macroscale measurements of contact angle. While no data are known to exist for contact angles on the small scales, nor for the dynamic conditions relevant to the growth or collapse cycle of bubble nucleation, of our experiments (i.e., advancing or receding contact angles), the hydrophobic nature of the treated surfaces was nonetheless evident in optical examination of microscale condensed dewdrops formed on a chilled device in a microscope. The droplets avoid the hydrophobic gold but form readily on hydrophilic gold.

**Thermal Transient Measurements.** A schematic of the experimental arrangement is shown in Figure 1b.

The portion concerning the bridge circuit and voltage measurement is similar to the arrangement described by Thomas et al.<sup>4</sup> The heater is connected to one leg of a Wheatstone bridge arrangement with 2 series resistors (15.1 Ω) and a variable resistor to balance the bridge. A pulse generator (Agilent 8114A<sup>16</sup>) is used to apply the voltage to the film, and a differential probe (Lecroy AP033<sup>16</sup>) is used to measure the Wheatstone bridge signal (the voltage difference between probe points) as described previously. A computer equipped with LabVIEW<sup>16</sup> was used to acquire  $V_{\text{measured}}$  and  $V_{\text{applied}}$  signals. Thermal transients were collected in filtered/deionized water (18 MΩ·cm) immediately before and after the laser flash microscopy experiments. The water was provided by a commercial filtering system (Barenstead/Thermolyne UV Deionization System, model D7331<sup>16</sup>).

An initial “burn-in” procedure was required to stabilize the measured resistance of the film. This involved applying a small voltage to the film (<1 V) and adjusting the variable resistor until a negligible voltage was observed. This is repeated until the resistance does not change. After the burn-in procedure the

resistance of the film was 2.7  $\Omega$ . In the experiments we report here, voltage pulses of 10.0 V were applied for 5  $\mu$ s at a frequency of 10 Hz. This is a somewhat arbitrary choice, as it is known that input power (i.e., input voltage) has a strong influence on surface heating rate.<sup>1</sup> The selection of a 10-V input pulse and 5- $\mu$ s heating time was made based on a combination of factors including the necessity of avoiding physical burnout of the heater, minimizing desorption of monolayers that is promoted by high temperatures and high-frequency operation, and keeping the physical size of the bubble within the optical field of view.

We were most interested in operating in the regime of homogeneous nucleation. As a result, the heater material (platinum) and thickness (0.2  $\mu$ m) were the same as used by Thomas et al.<sup>4</sup> who found that, when input power conditions were adjusted to produce a bubble approximately 3  $\mu$ s after initiation of a power pulse, the inflection-point temperature was very close to the predicted homogeneous nucleation temperature for water (about 300 °C). In the present experiments we also selected input parameters to produce inflection temperatures at about 3  $\mu$ s into the power pulse. Therefore, we infer that the mechanism for bubble nucleation is homogeneous for our experiments as well. Both heating and decay transients were recorded. Decay transients were collected by applying an offset baseline voltage (1 V) and measuring the evolution of output voltage across the bridge 10  $\mu$ s after the heating pulse was terminated.

The nucleation inflection times were calculated by finding the inflection point in the evolution of measured voltage. Specifically, the raw voltage data were smoothed with a graphing program (IGOR<sup>16</sup>) using a box function. The nucleation time was determined by calculating the minimum of the derivative curve.

**Laser Flash Microscopy.** The challenge in imaging is to record the bubble growth process with sufficient clarity to provide both qualitative and quantitative information on bubble morphology and growth rate. This requires images with minimal blurring. If  $R$  ( $\equiv dR/dt$ ) is the bubble growth rate and  $\Delta$  is the minimum physical distance that can be resolved in the visualization, then we require that  $\tau < \Delta/R$  for minimal blurring of the moving front, where  $\tau$  is the flash duration of the light source. Prior work imaged microboiling on small-diameter wires using pulse widths considerably longer than employed in the present work. For example, Skripov<sup>3</sup> imposed pulse widths of up to several hundred microseconds to induce explosive boiling of water on 20  $\mu$ m diameter platinum wires. At this level, the dynamics of phase change are considerably more accessible with commercial instrumentation, as shown by some of the images reported by Skripov<sup>3</sup> using 400-ns light flashes for illumination.

The much shorter pulse widths of interest in the present study—5  $\mu$ s—demand considerably shorter light flashes for imaging bubble morphology than have been previously used in photomicroscopy. For example, a typical bubble growth rate measured in our experiment is on the order of 0.03  $\mu$ m/ns, and the photomicroscopy arrangement we developed can resolve dimensions of about 0.5  $\mu$ m. A light flash would then have to be 17 ns in duration or less to “freeze” an event of this scale moving at this speed. On this basis, it is evident why illumination from light sources with pulse durations of 500 ns or longer, such as from a Xenon flash lamp, can produce significant blurring. To obtain a shorter light pulse, we illuminated the bubble growth process with a Nd:Yag laser with a flash duration (full width at half maximum) of 7.5 ns.

Our approach was to take one image at a specific time after initiation of the heating pulse. The growth process for a given surface condition and heating profile is then essentially pieced together from single images of individual events that are taken at progressively later times after the start of the heating pulse. In this way, we are able to record an effective bubble growth history at a framing rate of 100 million frames per second. The concern with this approach of constructing a growth history from different nucleation events is that the bubble morphology (size and shape) at any time after nucleation is repeatable for all events. Several fast transient thermal events undoubtedly have the requisite degree of repeatability to allow stringing images taken at successively later times after initiation to provide a picture of the entire event in one series (e.g., droplets splashing onto

solid surfaces<sup>17</sup>). In the present experiments, we assessed repeatability of the bubble dynamics for this purpose by holding the delay fixed and taking up to 20 images at the selected delay. Comparisons of the images showed bubble shapes that differed by no more than a few percent when layered one on top of another for the hydrophilic surfaces (bare Au and HDOH). Bubble collapse proved far less repeatable especially near the time of final collapse and disappearance of the bubble. For this reason, while we show complete representative growth/decay histories for selected bubble cycles, we report only quantitative data on the growth rate.

The low aspect ratio ( $1 \times 2$ ) of the heater allowed imaging the entire area of the heater with the microscope objective lens used. This advantage of imaging with low aspect ratio heaters came at the expense of inducing potentially significant temperature gradients along the imaged area during a heat pulse, as compared to high aspect ratio ( $\sim 100$ ) heaters as used in previous work (e.g., Thomas et al.<sup>4</sup>) where temperature gradients are negligible. This effect is expected to be more pronounced for platinum compared to a higher thermal conductivity material (e.g., aluminum). For this reason, we only report the raw Wheatstone bridge signal—output voltage. At the same time, the output voltage is proportional to temperature<sup>1,4</sup> so that we may be able to refer to features in the evolution of output voltage in the same way as evolution of average surface temperature, which is done in the subsequent discussions. Higher voltages imply higher average heater temperature and similarly for lower voltages. As noted previously, bubble nucleation was initiated by a voltage pulse of 10 V for 5  $\mu$ s. These conditions were selected to trigger nucleation nominally 2–3  $\mu$ s after initiation of the voltage pulse. We found that this choice allowed the phase change process to be visualized through a heating (pulse “on”) and cooling (pulse “off”) phase for all surface conditions examined.

In reference to Figure 1b, the components related to imaging include the following: Q-switched Nd:Yag laser light source (Surelite II<sup>16</sup> with the 1064-nm line frequency doubled to produce a 532-nm beam; the color of all images is green); Nikon Labophot II microscope<sup>16</sup> (with selected internal lens replaced with lenses that could withstand the high laser power) fitted with a 100X objective water immersion lens (Olympus<sup>16</sup> LUMPlanF1, 100X/1.00W,  $\infty/0$  objective lens); Nikon<sup>16</sup> D100 digital camera (with 6 MP resolution) for image capture; SRI<sup>16</sup> DG535 gate and delay generator to trigger the Q-switch and flash lamp of the laser; HP 8116A pulse generator for triggering an electrical pulse to the heater element; and a PC integrated with LabVIEW<sup>16</sup> control to allow systematically incrementing the delay between the Agilent<sup>16</sup> pulse generator, DG535 for the laser flash and camera shutter.

The images in all of our photographs were obtained by fixing the focus on the substrate. This had two effects. First, by fixing the focus on the base, we could operate the flash microscopy arrangement in Figure 1b in an automated mode where LabVIEW coordinates activating the sequence of events consisting of opening the shutter, then triggering the heating pulse and Q switch to expose the charge-coupled device (CCD) element of the camera, then repeating the process with a step delay on triggering the Q switch while keeping the other parameters fixed, and all through the DG535. This procedure significantly facilitates acquiring many photographs at progressively later delays and, thus, at later stages of bubble growth. Second, with a fixed focus on the base, a distinction between lateral growth along the surface and vertical growth into the bulk could be qualitatively assessed by noting the extent of image blurring. This will be further discussed later.

The camera shutter was open for 0.5 s to expose an image, but the room lighting was kept to a low value so as not to expose the CCD element prior to the laser flash. The camera was operated in “manual” mode. The ASA (American Standards Association) number was selected to optimize image quality for each set of operating conditions and averaged 800. Images were downloaded directly to the PC with a USB cable and viewed with the Nikon<sup>16</sup> Image Capture V 3.0 software. The time assigned to each image is accurate to within  $\pm 3.0$  ns, which is the “jitter” we measured

(17) Chandra, S.; Avedisian C. T. *Proc. R. Soc. London, Ser. A* **1991**, *A432*, 13–41.

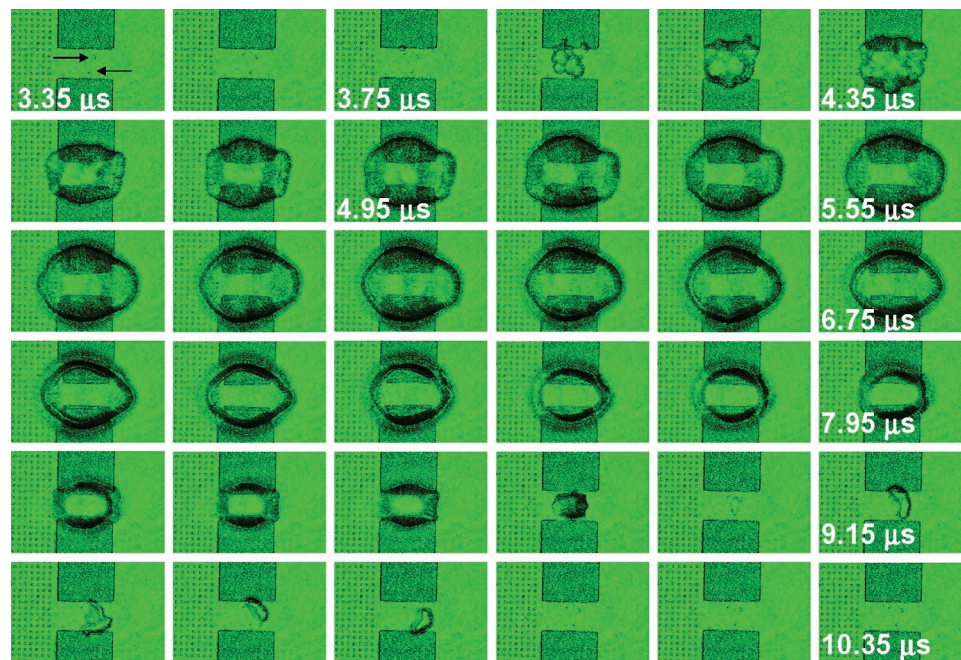


**Figure 2.** Laser flash microscopy on a bare Au film. The images were collected every  $0.1 \mu\text{s}$  beginning at time zero and continuing several microseconds past the conclusion of the  $5\text{-}\mu\text{s}$  heating pulse. For space considerations, the images shown begin near the first appearance of a bubble and continue in  $0.2\text{-}\mu\text{s}$  increments until the disappearance of vapor on the film. Heating conditions:  $10.0 \text{ V}$ ;  $5 \mu\text{s}$  in water.

that was associated with the appearance of the flash after triggering the Q switch.

The image quality was sensitive to the illumination intensity (which depends on the delay between the Q switch and flashlamp) and beam path to the microscope. A  $180\text{-}\mu\text{s}$  delay was used in the present experiments. The  $532\text{-nm}$  beam from the laser was directed to the universal illumination port of the microscope via a  $0.6\text{-mm}$  fiber optic cable attached to a collimator. The other end of the cable was positioned ahead of a  $25\text{-mm}$  plano-convex lens before the beam entered the microscope.

Physical dimensions of bubbles were obtained by transporting the digitized images to Image-Pro Plus software. Most of the bubbles were not spherical. For these bubbles, we determined an effective bubble radius by measuring the sides of a rectangle positioned around the bubble, and using the horizontal ( $W$ ) and vertical ( $H$ ) scales to obtain a sphere of equivalent radius as  $R_{\text{eq}} = (WH)^{1/2}$ . This approach was thought best in light of the often complex bubble shapes observed and the fact that our main interest was in determining a bubble growth rate ( $dR/dt$ ). For this purpose, an accurate measurement of time and an approximate measure of bubble size sufficed. Bubble radii were determined in this way only during the growth phase, especially the first  $1 \mu\text{s}$  and last  $2 \mu\text{s}$  of the  $5\text{-}\mu\text{s}$  pulse because of the aforementioned lack of repeatability of the bubble shape during collapse. The main source of uncertainty in the measurements was the blurred edge of the bubble boundary. To facilitate automating capture of a large number of images, we focused the lens on the substrate. The reader will see that in all of our photographs, the substrate is in focus. We also obtained a select number of images by focusing on the bubble periphery, which then makes the substrate blurred but the bubble edge in sharp focus, and found that our choice of the boundary of the bubble periphery for substrate focusing was within 5% of the value for periphery focusing.

For each surface condition (bare Au, HDOH (hydrophilic monolayer), HDT (hydrophobic monolayer)), the entire nucleation, growth, and collapse process was recorded for time steps of  $100 \text{ ns}$ . We also acquired images at the very beginning for each surface in  $10\text{-ns}$  steps. The finer time step images allowed us to examine more detailed features of the growth phase and to obtain more quantitative data on bubble growth. We have also assembled several collections of photographs into an effective movie sequence that covers the entire growth/collapse phase for hydrophobic and bare Au surfaces. These are discussed in the next section, along

with the reference to the movie sequences in the Supporting Information, which accompanies the text where the animations can be observed.

## Results and Discussion

**Visualization of Nucleation Events on Au Microheaters.** Figures 2–4 show laser strobe microscopy images as a function of time for bare gold, HDOH- (hydrophilic monolayer), and HDT-treated (hydrophobic monolayer) Au heaters. For clarity and space considerations, not all images collected are shown.

The time shown in the photographs is relative to the beginning of the heating pulse ( $0 \mu\text{s}$ ), which is  $5 \mu\text{s}$  in duration for all of our conditions. The grid of dots on the left side of the photographs of Figures 2–4 are wirebond pad “vias”. The arrows in Figures 2–4 indicate locations where surface imperfections were apparent in observation through the microscope. The nucleation behavior appeared to be independent of the defects, and in all cases the onset of nucleation occurred away from the defects. It is also noted from Figures 2–4 that bubbles are in focus only in the early stages of growth where they remain relatively close to the surface. At later times (e.g., after about  $4 \mu\text{s}$  in Figures 2–4), noticeable blurring of the bubble periphery is evident as the bubbles grow and move away from the focal plane (substrate). We elected not to refocus each image on the periphery, as we verified that the outer blurred edge of bubbles matched almost exactly the outer edges of bubble images re-focused on the bubble periphery for a given time. Two observations are apparent from these images.

First, the bubble nucleation/growth process shows no evidence of a growth/departure cycle at ready centers that is typical of nucleate boiling, where we define a “ready center” as a surface imperfection that could trap gas (e.g., a conical cavity). If such surface imperfections do exist on our surface, they are far too small to be observed except by atomic force microscopy scans of surface roughness. While we cannot confirm their presence on our heaters, we speculate on their influence for nucleation, which is

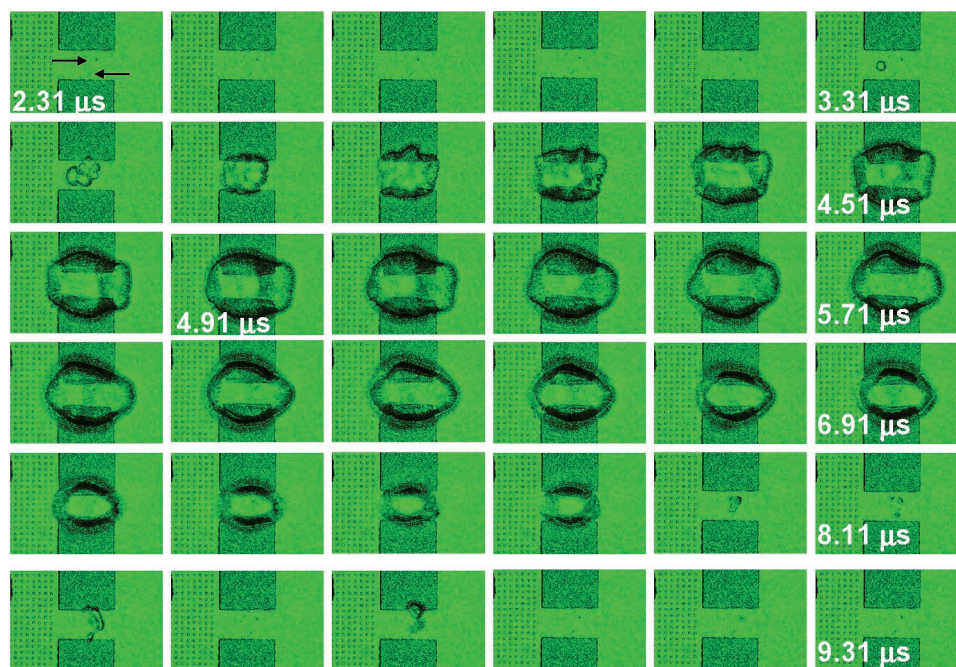


**Figure 3.** Laser flash microscopy on a HDOH-treated (hydrophilic monolayer) on Au. The images were collected every  $0.1 \mu\text{s}$  beginning at time zero and continuing several microseconds past the conclusion of the  $5\text{-}\mu\text{s}$  heating pulse. For space considerations, the images shown begin near the first appearance of a bubble and continue in  $0.2\text{-}\mu\text{s}$  increments until the disappearance of vapor on the film. Heating conditions:  $10.0 \text{ V}$ ;  $5 \mu\text{s}$  in water.

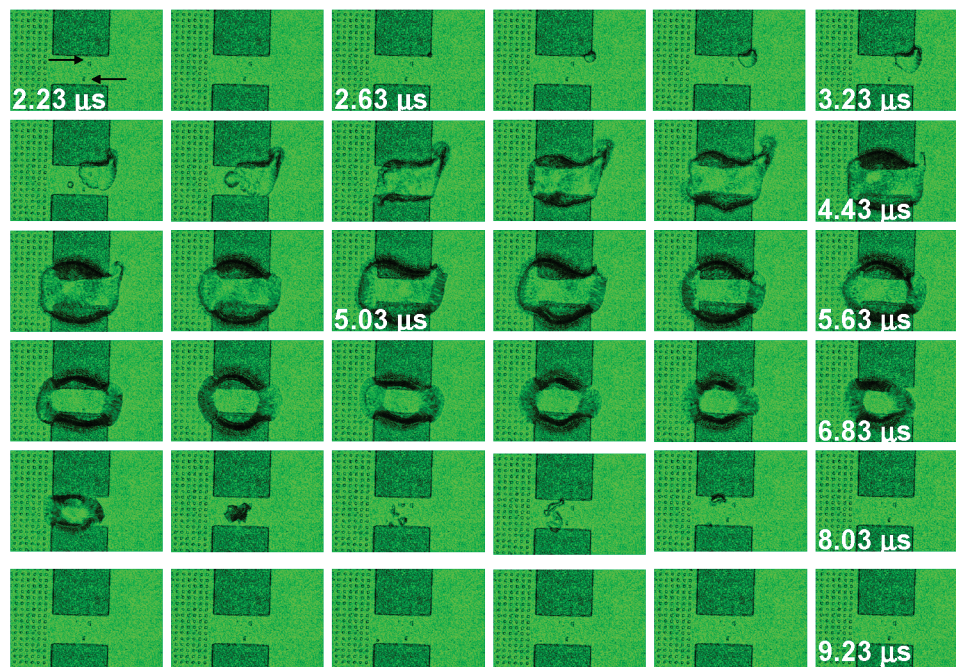


**Figure 4.** Laser flash microscopy on a HDT-treated (hydrophobic monolayer) on Au. The images were collected every  $0.1 \mu\text{s}$  beginning at time zero and continuing several microseconds past the conclusion of the  $5\text{-}\mu\text{s}$  heating pulse. For space considerations, the images shown begin near the first appearance of a bubble and continue in  $0.2\text{-}\mu\text{s}$  increments until the disappearance of vapor on the film. Heating conditions:  $10.0\text{ V}$ ;  $5 \mu\text{s}$  in water.

to contribute a partial pressure of noncondensable vapor ( $P_g$ ) to the total gas pressure in the bubble. With a ready center that traps gas, the nucleation process is still one of the bubble growing to a size where it is in metastable equilibrium with the surrounding liquid and with the vapor being comprised of molecules of the noncondensable gas and the surrounding liquid. The mechanism for the trapped gas can still be by molecular collisions at the liquid/vapor interface, even though there is a gas pocket present.

Second, the microbubbles continue to grow even after the heater is turned off (time  $> 5 \mu\text{s}$ ). This fact manifests

the significant inertia of the bubble, which increases the bubble size even during the cooling and collapse phase.

At this point, it is pertinent to mention the distinction between homogeneous nucleation at a surface and homogeneous nucleation in the bulk of a liquid,<sup>3,5</sup> because these processes can compete with each other when a liquid is in contact with a solid. The surface influences the bubble shape through the contact angle and the number of nucleation "sites", where by "sites" we essentially mean the number density of molecules. Surface wetting influences the contact angle, the volume of the bubble, and

threshold energy to form the bubble. Furthermore, at the solid/liquid interface the number of molecules/cm<sup>2</sup> is lower by a factor of  $N_o^{1/3}$  compared to the bulk number density (molecules/cm<sup>3</sup>),  $N_o$ . As a result, the surface nucleation rate  $J_s$  (nuclei/m<sup>2</sup>·s) is lower than the bulk rate  $J$  (nuclei/m<sup>3</sup>·s) by  $N_o^{1/3}$ . The competition between surface and bulk nucleation is then between the lower available “sites” at the surface compared to the bulk which would tend to make  $J_s < J$ , and the lower threshold energy at the surface compared to the bulk (due to a nonzero contact angle) which would make  $J_s > J$ . That hydrophobic surfaces with their higher contact angles produce lower superheats than hydrophilic surfaces attest to the general dominance of energy (and contact angle) considerations on the nucleation process. This trend is consistent with the present experiments and those of Thomas et al.<sup>4</sup> in which hydrophobic surfaces produced lower inflection point temperatures (and inflection point voltages in the present experiments) than hydrophilic surfaces.

In Figures 2 and 3, the first appearance of vapor occurs at 3.75 and 3.43  $\mu$ s, respectively. In each case the vapor continues to grow and extends beyond the length and width of the microheater. During the collapse phase, the vapor is present beyond 8  $\mu$ s or 3  $\mu$ s after the heating pulse has ended. The photographs in Figures 2 and 3 appear to indicate the reappearance of a bubble after a previous image shows no bubble. This is due to the variations observed in the collapse process from one pulse to the next; each image represents a separate pulse with a different delay setting between the voltage pulse and the laser flash. In contrast to the hydrophilic heaters, Figure 4 shows the images acquired from a hydrophobic heater. The first appearance of a bubble occurs earlier in the thermal transient for the hydrophobic case, at 2.63  $\mu$ s compared to the hydrophilic surfaces (HDOH SAM and bare Au substrate). The vapor phase is also present beyond the length of the heating pulse (5  $\mu$ s) but disappears at an earlier time than the hydrophilic cases.

In a previous studies,<sup>1,4</sup> surface thermal transients were correlated with the hydrophobic or hydrophilic nature of the surfaces. Properties of the transient such as nucleation time, nucleation temperature, and average temperature of the heater could be classified according to the wettability of the surface. Differences were observed in the nucleation behavior depending on the film’s wettability. HDOH-treated (hydrophilic monolayer) and bare Au heaters displayed similar behavior, while the HDT-treated (hydrophobic monolayer) heater displayed different characteristics. In the present study, since we now have direct optical access to the surface, we can examine the extent to which the inflection point signature in the surface temperature history coincides with the first appearance of bubbles at the surface.

Figure 5a compares the thermal transients for each surface preparation and shows representative photographs collected near the nucleation time calculated from the thermal transients data. At the inflection points in Figure 5a, the images in Figure 5b show the first appearance of a bubble. Figures 2–4 illustrate the complete growth sequence. The time for a nucleated bubble to completely cover the heater is on the order of 1  $\mu$ s, but the effect of the bubble on the surface temperature apparently is felt at much earlier times. Even for bubbles of the size shown in Figure 5b, the surface temperature appears to be effected as shown in Figure 5a thus supporting the contention that the inflection point indeed evidences bubble nucleation. For the unmodified, bare Au heater, the nucleation time (3.76  $\mu$ s) is nearly identical

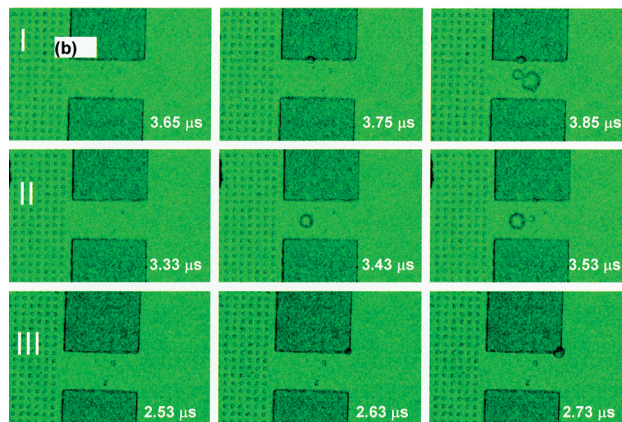
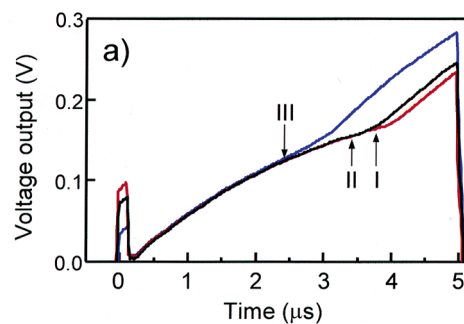


**Figure 5.** (a) Thermal transients for a bare Au film (I), hydrophilic SAM on Au (II), and a HDT-treated (hydrophobic monolayer) on Au (III). The arrows indicate the onset of nucleation. The voltage output is approximately proportional to heater temperature. (b) Laser flash microscopy images near the nucleation time recorded in part a. I, Au film; II, hydrophilic SAM on Au (II); III a HDT-treated (hydrophobic monolayer) on Au (III). Images were collected 0.1  $\mu$ s apart. Heating conditions are the same as in Figures 2–4.

to the time when vapor is first observed (3.75  $\mu$ s) and was reproducible throughout the entire experiment. This result is expected, since the surface wettability of a bare Au film is not expected to change during the experiment. In fact, the thermal transients collected over a time period of hours are repeatable and superimposable on each other (data not shown) indicative of a quasisteady temperature.

Figure 5b suggests the interesting phenomenon that bubbles are nucleating in the same area on the heater. On the other hand, for homogeneous nucleation we would have expected a more random placement of bubbles on the surface. We do not know enough about the nanoscale of the surface condition to know with certainty the reason for this localized nucleation process. It could be due to a combination of factors, including the presence of ready centers as discussed previously, to temperature gradients in the heaters we used compared to Thomas et al.<sup>4</sup> where the heaters were nearly isothermal because of the larger aspect ratio heaters used by Thomas et al. (50:1) compared to our heaters (2:1), or to the existence of nanobubbles. If the size of the gas pocket in the ready center is very small or if nanobubbles are present, the internal gas pressure and corresponding superheat of the metastable bubble would be large. Holmberg et al.<sup>18</sup> shows that nanobubbles are distributed over a larger region of the surface than what we see for the location of bubble nucleation in our experiments.

For the HDOH-treated (hydrophilic monolayer) heater, the appearance of vapor and the calculated nucleation

(18) Holmberg, M.; Kuhle, A.; Garnæs, J.; Mørch, K. A.; Boisen, A. *Langmuir* **2003**, *19*, 10510–10513.

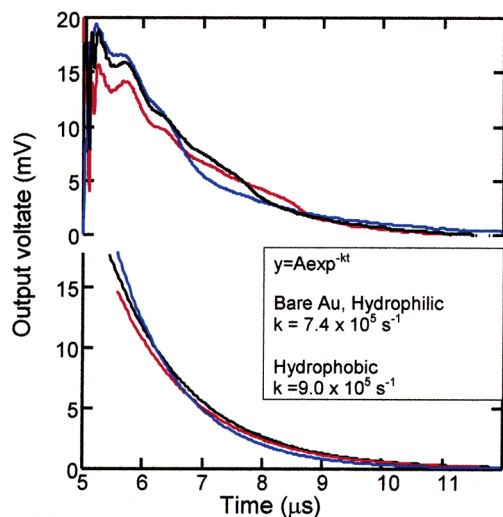


**Figure 6.** Top panel: decay thermal transients collected on bare Au film (red), hydrophilic SAM on Au (black), and a hydrophobic SAM on Au (blue). The voltage output is approximately proportional to heater temperature. The bottom panel gives exponential fits to the decay transients.

time before the laser flash microscopy differ by  $0.12 \mu\text{s}$  (the nucleation time is  $3.31$  vs  $3.43 \mu\text{s}$  by visual observation of vapor). However, the transient that was collected after the series of heating pulses for laser flash microscopy shows a shift in the nucleation time from  $3.31$  to  $3.43 \mu\text{s}$ . This shift suggests that a change in the surface wetting properties has occurred. Possible reasons for the change in wettability could be partial desorption of the monolayer from multiple heating pulses or by laser irradiation. Similar shifts in nucleation time and temperature were previously observed<sup>4</sup> and were attributed to gradual thermal desorption of the SAMs from repeated heating pulses. For the hydrophobic case, the nucleation time was  $2.40 \mu\text{s}$  before the laser microscopy and  $2.63 \mu\text{s}$  after the images were collected. The images indicate the vapor appearing at  $2.63 \mu\text{s}$ . The increase in nucleation time with increasing number of heating pulses is again consistent with previous results,<sup>4</sup> where the thermal transients for a hydrophobic monolayer changed over time and approached, but never reached, the characteristics for a bare Au film (nucleation temperature, time, average temperature) during a 2000-pulse experiment. In the experiments reported here, the total number of pulses applied to the film was  $<1000$  pulses depending on the number of images collected and the amount of time needed to focus the laser onto the surface.

We also acquired signals that illustrate the transient temperature during the decay phase of the growth/collapse process. Figure 6 shows representative decay voltage signals. The top panel displays the raw decay rate and the bottom panel contains exponential fits. The calculated decay rate was identical for the bare Au and hydrophilic SAM covered heaters. The hydrophobic SAM-modified heater exhibited a higher decay rate.

There appears to be enough energy in the fluidic system that, even after the heater pulse ends, the bubble continues to grow for another microsecond, as is evident in Figures 2 and 3. The heater, because it remains in thermal contact with liquid water for a longer time, does not rise to as high a final temperature, as shown in Figure 5. The decay transients in Figure 6 are consistent with this description of the hydrophobic heater beginning its decay from a higher temperature but decaying faster because of the smaller maximum bubble size and reduced energy in the fluidic system.

**Comparison of Growth Rates Between Hydrophilic and Hydrophobic Surfaces.** The phase change process can be broadly interpreted into two stages. In the first stage, bubble nucleation, occurs by molecular processes that create nuclei of the vapor phase; in the second stage, the bubble nuclei grow to produce a macroscopic phase transition. The processes governing these stages are fundamentally different, with the first stage controlled by random density fluctuations and the second determined by continuum processes associated with momentum and energy exchange.<sup>5</sup> The time scale of bubble nucleation is far shorter than the bubble growth time so that the thermodynamic state of first visible appearance of the bubble essentially corresponds to the nucleation state. As noted above, the nucleation temperature can be determined by an inflection point in the surface temperature.<sup>1</sup> In the experiments described here, the bubbles are already of essentially macroscopic size when first observed, and the phase change process is already in the growth phase.

Quantitative measurements of the bubble equivalent diameter,  $D_{\text{eq}}$ , showed a bubble growth process that was roughly consistent with trends from classical bubble growth theory.<sup>5</sup> By use of this theory, the growth law for the bubble radius ( $R = D_{\text{eq}}/2$ ) can be represented by a power law in time as  $R \approx t^n$  where  $0 < n < 1$ . Almost immediately after nucleation, the bubble starts to grow as the pressure in the bubble overcomes the surface tension force ( $2\sigma/R$ ) where  $\sigma$  is the liquid/vapor surface tension. Heat transfer plays no role. As the bubble grows and  $2\sigma/R$  decreases, the vapor in the bubble cools because the gas temperature tracks with the internal pressure inside the bubble (approximately) along the saturation curve. The increasing temperature difference takes over as a controlling mechanism for bubble growth, and the growth process is the result of mass transfer into the bubble by evaporation at the liquid/vapor interface caused by heat transfer from the far field surrounding liquid to the bubble wall. For bubble growth controlled by heat transfer,  $n = 1/2$ ; for bubble growth controlled by inertia,  $n = 1$ .

Figures 7–9 show plots of  $D_{\text{eq}}$  as a function of time after initial nucleation, obtained from bare Au, HDOH-modified, and HDT modified heaters, respectively. Also shown are curve fits of the data using a power-law relationship,  $R \approx t^n$  as suggested by the classical theory of bubble growth.<sup>5,19</sup> For the bare gold and HDOH-treated (hydrophilic monolayer) cases, there was a limited time range over which growth could be characterized. Within 100 ns of nucleation, neighboring bubbles would begin to make contact, so that it was impossible to follow the growth of a single bubble for longer times. The effective framing rate of the sequences shown in Figures 7 and 8, for which images were acquired at 10-ns intervals, is about 100 million frames/s.

The hydrophobic SAM (Figure 9) allowed for a wider time range for growth characterization, but quantitative analysis was complicated by the nonspherical shape of the bubble. The bubbles consistently nucleated in the corners as shown in Figure 9 then grew into the heater footprint, with a segment also penetrating upward. To determine an effective bubble diameter for this case, we arbitrarily divided the bubble into two portions, surrounded each portion with its own rectangular box, and then added the two areas to determine the effective bubble diameter (by the approach described previously). One portion corresponded to part of the phase boundary that grew upward around the corner as shown in Figure 9, and the other grew laterally to cover the heater footprint.

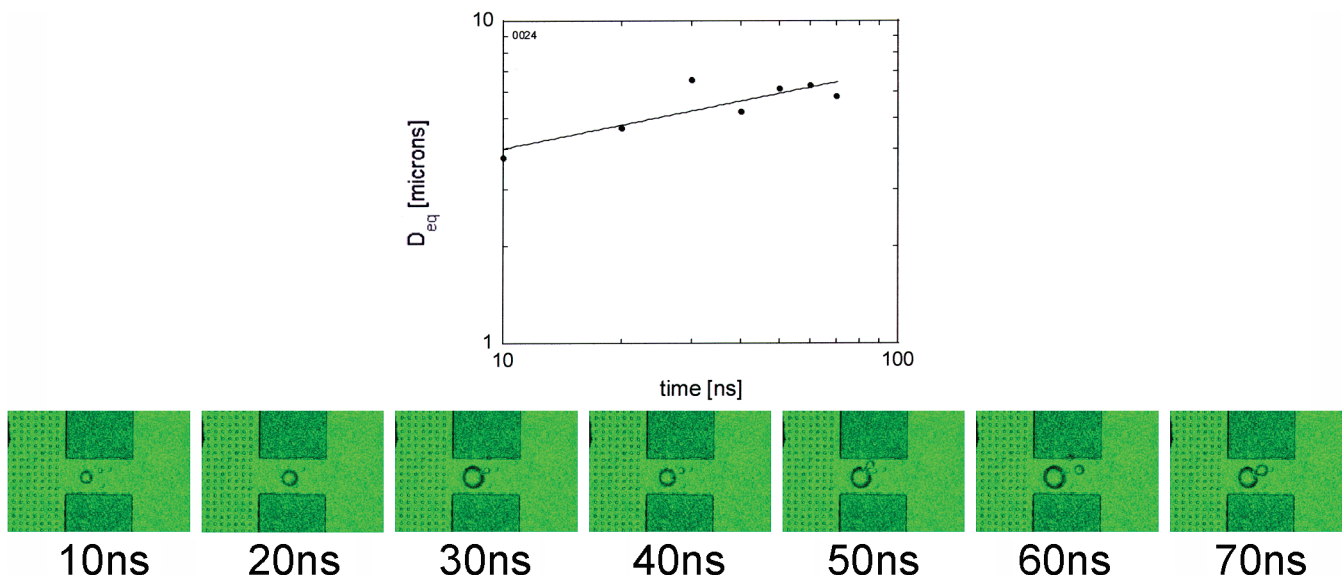


**Figure 7.** Change in bubble size as a function of time after initial nucleation for the bare Au surface. The solid line is a power-law fit to the data ( $R \approx t^n$ ), with parameters of the fit given in Table 1. Also shown are the images used for each data point. Time after nucleation is indicated beneath each photograph.

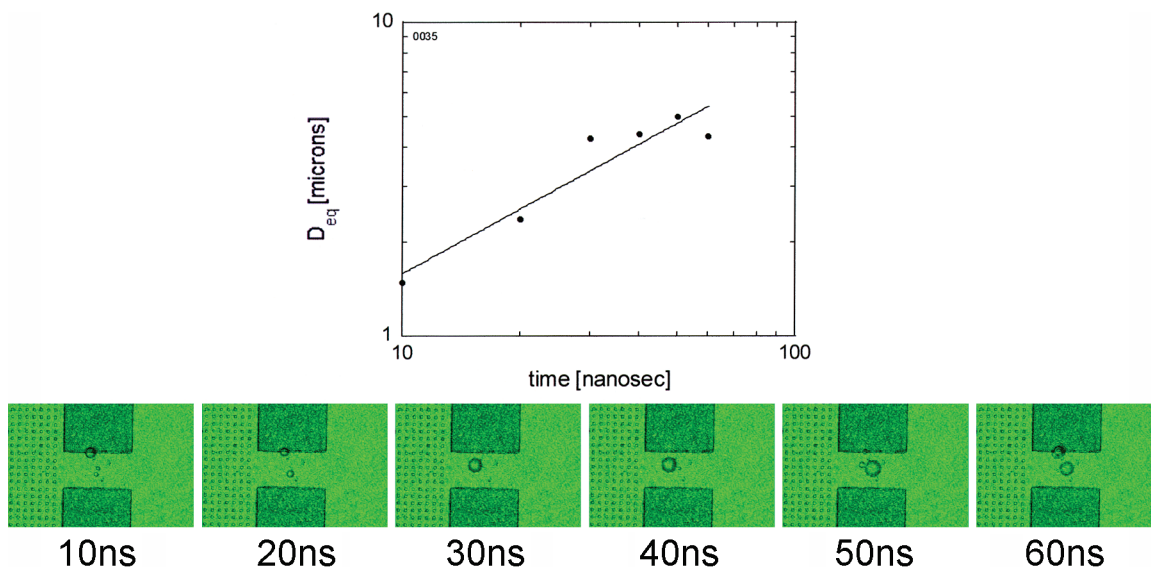


**Figure 8.** Change in bubble size as a function of time after initial nucleation for HDOH (hydrophilic monolayer) surface. The solid line is a power-law fit to the data ( $R \approx t^n$ ), with parameters of the fit given in Table 1. Also shown are the images used for each data point. Time after nucleation is indicated beneath each photograph.

During the lateral growth phase in which the bubbles cover the heater before growing away from the surface, the bubble surface exhibits a nonsmooth and somewhat ruffled appearance with some evidence of an instability at the boundary. This is shown in Figures 2–4 in the early period of growth. Figure 10 displays a bubble image taken 400 ns after nucleation for the HDT surface of Figure 9.

Surface distortions are evident on the left side of the bubble that spreads over the heater footprint. The distortions appear to be similar to the instabilities observed in explosive boiling of ether droplets suspended in glycerine at the superheat limit, though here on a much smaller physical scale. The origin of surface instabilities for suspended droplets was speculated<sup>20,21</sup> to be due to a baroclinic Landau–Darrius instability mechanism of

planar laminar flames, with triggering of the instability apparently being accomplished by a mechanism similar to flow over a flat plate which triggers a transition to turbulence. Furthermore, the temperature of the liquid/vapor interface for the case of exploding droplets was predicted to be between the saturation temperature of the liquid and bulk liquid temperature.

Measurements of the equivalent diameter in Table 1 show that power “ $n$ ” is consistent with the classical theory of bubble growth with a value that ranges between the extremes of inertially and thermally controlled growth.<sup>5,19</sup> Also listed in Table 1 is an average bubble growth rate (based on a linearized correlation). The bubble growth rates range between 16 and 64 m/s. This range is consistent with jet velocities for explosive boiling of suspended organic liquid droplets at atmospheric pressure.<sup>20</sup> This comparison lends support to extending the mechanism speculated for surface instabilities of exploding droplets to the interface wrinkling observed here for rapid evaporation on pulse

(20) Frost, D. L.; Sturtevant, B. J. *Heat Transfer* **1986**, *108*, 418–424.

(21) Frost, D. L. *Phys. Fluids* **1988**, *31*, 2554–2561.

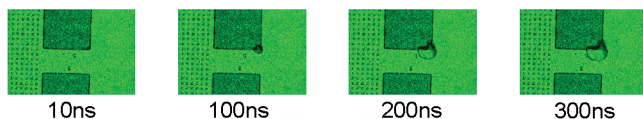
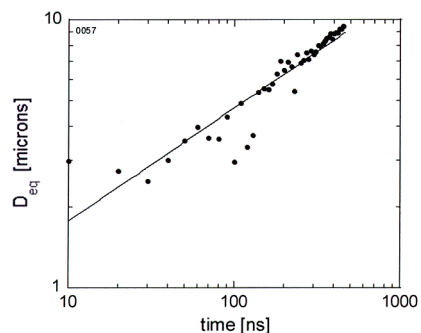


**Figure 9.** Change in bubble size as a function of time after initial nucleation for the HDT (hydrophobic monolayer) surface. The solid line is a power-law fit to the data ( $R \approx t^n$ ), with parameters of the fit given in Table 1. Also shown are the images used for selected data points. Time after nucleation is indicated beneath each photograph.

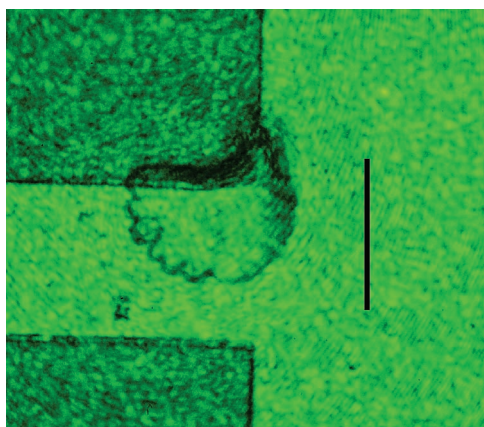


**Figure 10.** Photograph of a bubble 400 ns after nucleation for the HDT (hydrophobic monolayer) surface of Figure 9. The vertical line measures 15  $\mu\text{m}$ . The photograph illustrates surface instabilities on the bubble perimeter.

heated thin films. It is also evident from Table 1 that the bubble growth rate is lowest for the hydrophobic SAM, which is consistent with the lower nucleation temperature and thus reduced heat transport to the bubble compared to a hydrophilic SAM.

### Conclusions

The nucleation, growth, and collapse of rapidly heated bubbles have been characterized on gold microheaters with

**Table 1. Bubble Growth Exponent ( $n$ ) and Growth Rate ( $\dot{R}$ ) from Figures 7–9**

surface	$n$	$\dot{R}$ ( $\mu\text{m}/\text{ns}$ )
HDOH-treated (hydrophilic monolayer)	0.24	0.033
bare gold	0.69	0.064
HDT-treated (hydrophobic monolayer)	0.42	0.016

prepared surfaces of varying hydrophobicity. By use of a novel laser-strobe microphotography technique, images of the different stages of the process were collected. Data from electrical transients (i.e., output voltage) corresponding to changes in the microheater temperature and, thus, electrical resistivity were also collected and supported the results of the imaging. It was found that the same 5- $\mu\text{s}$  pulse (short enough for superheating of the liquid to occur) applied to the differently prepared heaters produced significant differences of temperature and bubble morphology among the surfaces. The HDT hydrophobic surface produced a bubble that nucleated at an earlier time, grew more slowly to a smaller maximum size, exhibited significant surface instabilities during growth, and collapsed more rapidly than bubbles formed on bare gold and HDOH-treated (hydrophilic monolayer) surfaces. Output voltages (i.e., surface temperatures) were higher for hydrophilic surfaces compared to hydrophobic surfaces, which is consistent with a smaller contact angle for the hydrophilic surface and, thus, more spherical bubble and larger superheat. The results also indicate the advantages of laser flash photomicroscopy for high temporal resolution of imaging phase change processes at a few microseconds duration.

**Acknowledgment.** K.M.B. acknowledges the NIST National Research Council Postdoctoral program; C.T.A. acknowledges support from NIST through an IPA agreement with Cornell University. The authors also greatly benefited from discussions and assistance with Drs. Joseph Hodges, Cary Presser, and John Suehle and from Mr. Christopher Montgomery for wire bonding and general technical assistance with microheaters.

**Supporting Information Available:** Collections of photographs assembled into an effective movie sequence that covers the entire growth/collapse phase for hydrophobic and bare Au surfaces. This material is available free of charge via the Internet at <http://pubs.acs.org>.

LA040137T